H^2GM: A Hierarchical Hypergraph Matching Framework for Brain Landmark Alignment

Zhibin He[1], Wuyang Li[3], Tuo Zhang[1(✉)], and Yixuan Yuan[2(✉)]

[1] School of Automation, Northwestern Polytechnical University, Xi'an, China
tuozhang@nwpu.edu.cn
[2] Department of Electronic Engineering, The Chinese University of Hong Kong, Shatin, Hong Kong SAR, China
yxyuan@ee.cuhk.edu.hk
[3] Department of Electrical Engineering, City University of Hong Kong, Kowloon, Hong Kong SAR, China

Abstract. Gyral hinges (GHs) are novel brain gyrus landmarks, and their precise alignment is crucial for understanding the relationship between brain structure and function. However, accurate and robust GH alignment is challenging due to the massive cortical morphological variations of GHs between subjects. Previous studies typically construct a single-scale graph to model the GHs relations and deploy the graph matching algorithms for GH alignment but suffer from two overlooked deficiencies. First, they consider only pairwise relations between GHs, ignoring that their relations are highly complex. Second, they only consider the point scale for graph-based GH alignment, which introduces several alignment errors on small-scaled regions. To overcome these deficiencies, we propose a Hierarchical HyperGraph Matching (H^2GM) framework for GH alignment, consisting of a Multi-scale Hypergraph Establishment (MsHE) module, a Multi-scale Hypergraph Matching (MsHM) module, and an Inter-Scale Consistency (ISC) constraint. Specifically, the MsHE module constructs multi-scale hypergraphs by utilizing abundant biological evidence and models high-order relations between GHs at different scales. The MsHM module matches hypergraph pairs at each scale to entangle a robust GH alignment with multi-scale high-order cues. And the ISC constraint incorporates inter-scale semantic consistency to encourage the agreement of multi-scale knowledge. Experimental results demonstrate that the H^2GM improves GH alignment remarkably and outperforms state-of-the-art methods. The code is available at here.

Keywords: Graph matching · Point cloud registration · Hypergraph

Z. He—This work was done when Zhibin He was a visiting student at the Department of Electronic Engineering, The Chinese University of Hong Kong.

H. Greenspan et al. (Eds.): MICCAI 2023, LNCS 14229, pp. 548–558, 2023.
https://doi.org/10.1007/978-3-031-43999-5_52

1 Introduction

The ultimate goal of entire cortex registration (ECR) is to achieve functional region alignment across subjects. However, existing software often sacrifices the local functional alignment accuracy to accomplish ECR [6]. Previous studies have identified a novel brain gyrus landmark, termed the gyral hinge (GH) [10,13,30]. It has been demonstrated that the precise GH alignment over the whole brain is critical for understanding the relationship between brain structure and function [16]. However, achieving accurate and robust GH alignment is challenging due to the massive cortical morphological variations in GHs between subjects [9,16].

To address this issue, existing works have introduced the single-scale graph structure to represent and align GHs [16,29,31]. As shown in Fig. 1(a), they model GHs as graph nodes, formulate graph edges with the white matter fiber connections between GHs, and deploy the graph matching algorithms to align GHs [29,31]. Despite the great successes, existing works suffer from two overlooked deficiencies. First, they consider only pairwise relations between GHs to construct graphs that use second-order edges (the one-hop connection between two GHs), without considering underlying complex (e.g., high-order) relations among more than two GHs [23,28]. For example, the high-order relations of GHs within the same brain region cannot be well modeled only in low-order cues [5]. Hence, we are committed to going beyond the second-order relations and seeking a more effective graph structure, hypergraph, to model such high-order relations [2,15,26,32]. Second, existing works focus only on a single-scale, *i.e.,* the point scale [16,29,31], ignoring the hierarchy of brain structure and function at multiple scales [1]. Only considering the single-scale knowledge is insufficient to capture the multi-scale dependence within graphs, inevitably introducing several alignment errors on small-scaled regions [3]. Hence, we aim to introduce multi-scale knowledge in hypergraph matching (Fig. 1(b)), exploring more effective message propagation with hierarchical hypergraph learning.

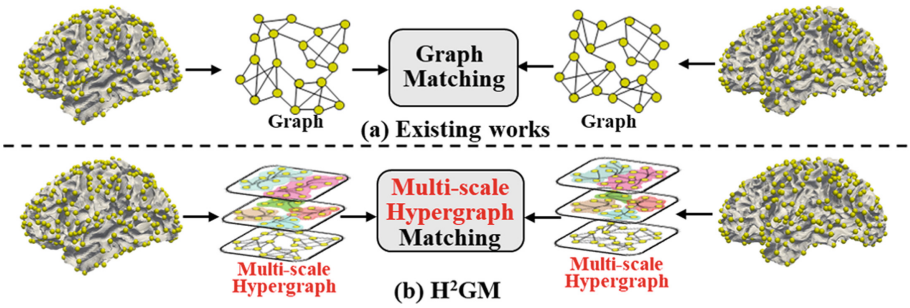

Fig. 1. Illustration of the GH alignment. (a) Previous works use graph structure to represent and align GHs at a single scale. (b) The proposed H²GM introduces multi-scale hypergraph matching for a better GH alignment.

To overcome the aforementioned challenges, we propose a Hierarchical Hyper-Graph Matching (H^2GM) framework for GH alignment, which consists of a Multi-scale Hypergraph Establishment (MsHE), a Multi-scale Hypergraph Matching (MsHM), and an Inter-Scale Consistency (ISC) constraint. Specifically, in the MsHE module, we construct multi-scale hypergraphs with three hierarchical scales (Five Lobes Atlas, DK Atlas [4], GH) and establish correspondences for both inter-scale and inter-subject hypergraphs. As for the MsHM module, we match the hypergraph pairs at each scale to entangle a robust GH alignment with multi-scale high-order cues. Finally, ISC incorporates inter-scale semantic consistency to encourage the agreement of multi-scale knowledge. Experimental results demonstrate that our framework enables more effective GH alignment. In summary, the main contributions are as follows: (1) We propose a H^2GM framework for GH alignment. To the best of our knowledge, this work is the first attempt to leverage multi-scale hypergraphs to align the brain landmark. (2) We design a MsHE module to extract the high-order relations among GHs at different scales and a MsHM module to propagate GHs features to align GHs. Moreover, the feature distribution of GH optimized by the inter-scale semantic consistency further improves the alignment accuracy. (3) Extensive experiments verify that the proposed matching framework improves the GH alignment remarkably and outperforms state-of-the-art methods.

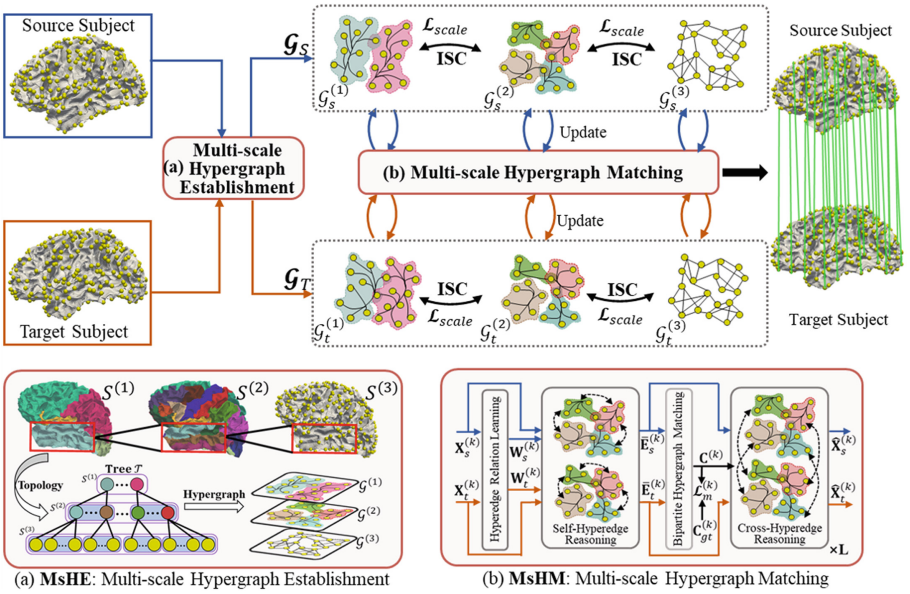

Fig. 2. Overview of the proposed H^2GM. ISC represents inter-scale consistency.

2 Method

The overview of our proposed framework is shown in Fig. 2, which contains two parts. Given two subjects MRI, we extract GHs and establish multi-scale hypergraphs $\mathcal{G}_{s/t}^{(k)} = \left\{\mathbf{H}_{s/t}^{(k)}, \mathbf{X}_{s/t}^{(k)}, \mathbf{W}_{s/t}^{(k)}\right\}$ in the MsHE module (Fig. 2(a)), illustrated in Sect. 2.1. Then we perform multi-scale GH alignment in the MsHM module (Fig. 2(b)) to obtain multi-scale correspondence matrix $\mathbf{C}^{(k)}$ (Sect. 2.2). The $\mathbf{C}^{(k)}$ indicating the correspondence between two hypergraphs, *i.e.*, $\mathbf{C}_{i,j}^{(k)} = 1$ means the i-th GH in source matches to the j-th GH in target at the k scale. The GH alignment can be formulated as the hypergraph matching problem:

$$\min_{\theta} g(\theta) = \min_{\theta} \sum_{k=1}^{K} \left(\mathbf{H}_s^{(k)\,T} \mathbf{X}_s^{(k)} - \mathbf{C}^{(k)} \mathbf{H}_t^{(k)\,T} \mathbf{X}_t^{(k)} \mathbf{C}^{(k)\,T} \right), \tag{1}$$

where θ represents the neural network parameters, the $\mathbf{H}$ is the incidence matrix of hypergraph [5], the $\mathbf{X}$ is the GHs' features, and the k is the number of scale. We use a neural network to predict $\mathbf{C}^{(k)}$. The details will be introduced below.

2.1 Multi-scale Hypergraph Establishment (MsHE)

As shown in Fig. 2(a), we utilize the Five Lobes Atlas, DK Atlas [4], and GH as three scales to model the inter-scale relations through a tree structure $\mathcal{T}$ [3]. In the tree structure $\mathcal{T}$, the larger-scale brain regions are parent nodes, and the smaller-scale brain regions or GHs are child nodes. As for the multi-scale hypergraph incidence matrix $\mathbf{H}_{s/t}^{(k)}$, we capture the topological relations among brain atlases to serve as the incidence matrix. The element $\mathbf{H}_{i,j}^{(k)}$ indicates that the i-th GH is included in the j-th hyperedge (brain region or GH). Notably, when k=3, the row sum of $\mathbf{H}_{s/t}^{(k)}$ is 1 and $\mathbf{H}_{s/t}^{(k)}$ is in the diagonal format. As for the hypergraph nodes $\mathbf{V}_{s/t}$, *i.e.*, GHs, we capture various cues in the subject to serve as the raw node feature. Specifically, considering the limited representation of the single vertex knowledge, we expand each GH on the surface by two rings, resulting in a total of 19 vertices as the GHs' raw features. Each vertex features contain three-dimensional coordinates ($\times$3), normal vector coordinates ($\times$3), curvature ($\times$1), convexity ($\times$1), and cortical thickness ($\times$1). Then, the aforementioned features are contacted to obtain the raw node features $\mathbf{V}_{s/t}^{(k)} \in \mathbb{R}^{m/n \times d}$, where m/n represent the number of source/target subject GHs, respectively. After that, the raw features are sent to Dynamic Graph CNN [25] (DGCNN) to extract GHs descriptors $\mathbf{X}_{s/t}^{(k)} \in \mathbb{R}^{m/n \times D}$ as the final node representation. Notably, the parameters of the DGCNN are shared across all scales. For the hyperedge weight matrix $\mathbf{W}_{s/t}^{(k)}$, we propose to use a diagonal metric with one-value entries as the initialization, which will be optimized in the following hyperedge relation learning module. Finally, we obtain the multi-scale hypergraphs of source/target subjects as $\mathcal{G}_{s/t}^{(k)} = \left\{\mathbf{H}_{s/t}^{(k)}, \mathbf{X}_{s/t}^{(k)}, \mathbf{W}_{s/t}^{(k)}\right\}$. The proposed multi-scale hypergraphs can well model significant surface morphological information and multi-scale GH relations for better GH alignment.

2.2 Multi-scale Hypergraph Matching (MsHM)

As shown in Fig. 2(b), the hyperedge features at k scale are computed as $\mathbf{E}_{s/t}^{(k)} = \mathbf{H}_{s/t}^{(k)\,T}\mathbf{X}_{s/t}^{(k)}$, and then sent to MsHM to solve the multi-scale matching with four sub-stages, including hyperedge relation learning, self-hyperedge reasoning, bipartite hypergraph matching, and cross-hyperedge reasoning.

Hyperedge Relation Learning: To dynamically learn hyperedge relation with better structural information, we propose hyperedge relation learning to model the high-order relation among hyperedges, instead of directly using the handcraft hyperedge weight metric $\mathbf{W}_{s/t}$ [5,15]. The layer utilizes transformer [7,22], which comprises several encoder-decoder layers, to generate hyperedge soft edges. Specifically, the transformer takes hyperedge features $\mathbf{E}_{s/t}$ as input and encodes them into embedding features. The inner product of these embedded features is then passed through a softmax function to generate the hyperedge weight matrices. This process can be expressed as follows:

$$\mathbf{W}_{s/t}^{(k)} = softmax((f_{emb}(\mathbf{E}_{s/t}^{(k)}))^T, f_{emb}(\mathbf{E}_{s/t}^{(k)}), \tag{2}$$

where f_{emb} is a transformer-based feature embedding function.

Self-hyperedge Reasoning: We utilize a self-hyperedge reasoning network to capture the self-correlation of hyperedge features. Propagating features achieve this by hyperedge weight matrix within each hypergraph. It can be written as:

$$\bar{\mathbf{E}}_{s/t}^{(k)} = \sigma\left(\mathbf{W}_{s/t}^{(k)}\mathbf{E}_{s/t}^{(k)}\mathbf{\Theta}_{s/t}^{(k)}\right), \tag{3}$$

where $\mathbf{\Theta}_{s/t}^{(k)} \in \mathbb{R}^{D\times D}$ denotes the learnable parameters of self-hyperedge reasoning network. And $\sigma(\cdot)$ is the nonlinear activation function.

Bipartite Hypergraph Matching: We use bipartite matching to determine a soft correspondence matrix between two subjects, which is achieved using the following expression: $\mathbf{C}^{(k)} = \text{Gbm}\left(\bar{\mathbf{E}}_s^{(k)}, \bar{\mathbf{E}}_t^{(k)}\right)$, where Gbm consists of an Affinity layer, an Instance normalization layer, a quadratic constrain (QC) layer, and a Sinkhorn layer. Initially, the affinity matrix is computed as $\mathbf{A}^{(k)} = \bar{\mathbf{E}}_s^{(k)}\mathbf{M}^{(k)}\bar{\mathbf{E}}_t^{(k)}$, where $\mathbf{M}^{(k)} \in \mathbb{R}^{D\times D}$ is the learnable parameter matrix in the affinity layer. Next, we apply instance normalization [20] to transform $\mathbf{A}^{(k)}$ into a matrix with positive elements within finite values. We then introduce QC to minimize the structural difference of matched GH pairs [8,14]. For unmatched GHs, we add an additional row and column of ones to the output of the QC layer matrix, which is then processed through the Sinkhorn layer [19] to obtain a double-stochastic affinity matrix with maximum iteration optimization. After deleting the added

row and column, we obtain a soft assignment matrix $\mathbf{C}^{(k)}$. Finally, we use cross-entropy-type loss functions to compute the linear assignment cost between the ground truth and the soft assignment matrix, which is defined as follows:

$$\mathcal{L}_m = \sum_{k=1}^{K} \left(\sum_{l=1}^{L} \left(\mathbf{C}_{gt}^{(k)} \log \left(\mathbf{C}_{l}^{(k)} \right) + \left(1 - \mathbf{C}_{gt}^{(k)} \right) \log \left(1 - \mathbf{C}_{l}^{(k)} \right) \right) \right), \tag{4}$$

where $\mathbf{C}_{gt}^{(k)} \in \{0, 1\}, \mathbf{C}_{l}^{(k)} \in [0, 1]$, and this loss can optimize the Eq. 1. The k-scale soft assignment matrix of the MsHM l-th layer output is $\mathbf{C}_{l}^{(k)}$.

Cross-Hyperedge Reasoning: We further enhance the hyperedge features by exploring cross-correlation through cross-hyperedge reasoning. Different from self-hyperedge reasoning, the proposed cross-hyperedge reasoning enables subject-aware message propagation, facilitating effective interaction between subjects. The more similar a pair of hyperedges is between two subjects, the better features will be aggregated in better alignment. It can be written as:

$$\hat{\mathbf{E}}_{s/t}^{(k)} = f_{cross} \left(\bar{\mathbf{E}}_{s/t}^{(k)}, \mathbf{C}^{(k)} \bar{\mathbf{E}}_{t/s}^{(k)} \right), \tag{5}$$

where f_{cross} consists of a feature concatenate and a fully connected layer. Finally, the new GHs features with a symmetric normalization can be written as:

$$\mathbf{X}_{s/t}^{(k)} = \sigma((\mathbf{D}_{s/t}^{(k)})^{-1} \mathbf{H}_{s/t}^{(k)} \mathbf{W}_{s/t}^{(k)} (\mathbf{B}_{s/t}^{(k)})^{-1} \hat{\mathbf{E}}_{s/t}^{(k)} \mathbf{\Phi}_{s/t}^{(k)}), \tag{6}$$

where $\sigma(\cdot)$ is the nonlinear activation function. $\mathbf{D}_{s/t}^{(k)}$ and $\mathbf{B}_{s/t}^{(k)}$ are the diagonal node degree matrix and hyperedge degree matrix, respectively. $\mathbf{\Phi} \in \mathbb{R}^{D \times D}$ denotes the learnable parameters of cross-hyperedge reasoning network.

2.3 Inter-Scale Consistency (ISC)

To avoid the potential disagreement among different scales, it is critical to introduce the consistency constraint across scales, which achieves collaborative optimization in different scales and prevents sub-optimal alignment. Specifically, we propose a novel ISC mechanism that leverages the local properties of the tree structure. For a parent hyperedge $\boldsymbol{e}_p$ and its child hyperedges $\{\boldsymbol{e}_c^q\}_{q=1}^{Q}$ (Q is the number of children nodes belonging to the same parent node.), which represent the same brain region at different scales, we enforce semantic-level consistency between the child hyperedges and their parent hyperedge to facility the reliable model learning, which is denoted as follows:

$$\mathcal{L}_{\text{scale}} = \sum_{\forall \mathcal{T}_{s/t}} \left\| \boldsymbol{e}_p - \sum_{q=1}^{Q} \boldsymbol{e}_c^q \right\|^2, \tag{7}$$

where $\mathcal{L}_{\text{scale}}$ denotes the loss function that enforces inter-scale semantic consistency among source/target subjects tree structure $\mathcal{T}_{s/t}$. By incorporating this loss, the model learns to maintain consistent semantic information across different scales for hyperedges corresponding to the same brain region.

2.4 Model Optimization

In the training of this work, we introduce a hyperparameter to add up $\mathcal{L}_m$ and $\mathcal{L}_{scale}$. Then, the overall train loss for the GH alignment model is denoted as:

$$\mathcal{L} = \mathcal{L}_m + \beta \mathcal{L}_{scale}, \tag{8}$$

where β is a hyperparameter to control the intensity. In testing, we utilize the Hungarian algorithm [12] to convert the soft assignment matrix into a binary matrix. Subsequently, the rows and columns of the binary matrix with a value of 1 represent the GHs correspondences between source and target subjects.

Table 1. Comparison with state-of-the-art methods and the ablation studies on the GH alignment dataset. The best performance is highlighted in bold.

Method	Accuracy (%)	Correlation	MGE
Ground Truth	100	39.84 ± 3.83	0
SurfReg [6]	\	27.67 ± 4.93	\
HNN (AAAI2019) [5]	77.10 ± 8.53	37.01 ± 3.96	6.7
PCA-GM (ICCV2019) [24]	74.32 ± 8.55	35.50 ± 4.07	10.1
RGM (CVPR2021) [7]	74.71 ± 8.67	35.85 ± 4.03	9.7
QC-DGM (CVPR2021) [8]	71.83 ± 9.74	34.72 ± 4.26	11.2
REGTR (CVPR2022) [27]	75.30 ± 8.31	36.30 ± 3.97	8.8
Sigma++ (TPAMI2023) [15]	77.01 ± 8.41	36.98 ± 3.96	6.7
w/o ISC	77.66 ± 8.27	37.83 ± 3.93	6.2
w/o Multi-scale	74.81 ± 8.66	35.92 ± 4.02	9.6
w/o Hyperedge Relation Learning	77.43 ± 8.28	37.79 ± 3.93	6.5
Our (H^2GM)	$\mathbf{78.03 \pm 8.21}$	$\mathbf{37.99 \pm 3.91}$	**5.8**

3 Experiments and Results

3.1 Experimental Setup

Dataset: We evaluate our proposed framework effectiveness by conducting experiments on the GH alignment dataset, which includes the ground truth of GH correspondences across 250 subjects. Each GH contains brain atlas information, various morphological features from T1-weighted (T1w) MRI, and task activation vectors obtained from the task fMRI (tfMRI). The Five Lobe Atlas consists of 10 brain regions, while the DK Atlas includes 66 brain regions. The T1w MRI and tfMRI are acquired from the WU-Minn Human Connectome Project (HCP) consortium [21], with written informed consent obtained from HCP participants and relevant institutional review boards approving the study.

Evaluation: In this study, we adopt the accuracy, the correlation ($\times 10^{-2}$), and the mean geodesic errors [17] (MGE, in centimeters) as evaluation metrics for our proposed model. Specifically, accuracy is computed as the average rate of correct GH alignments across all subjects. Furthermore, we use correlation to measure the similarity between the activation vectors of the aligned GH pairs across all subjects. The higher the value of correlation, the higher the confidence that the two GHs align correctly. To evaluate the performance of our model, we compare it against several state-of-the-art learning-based point cloud registration methods, including RGM [7], QC-DGM [8], and REGTR [27], as well as several learning-based graph matching methods, including HNN [5], PCA-GM [24], and Sigma++ [15], and the traditional surface registration method, SurfReg [6]. Notably, we exclude comparisons with non-open-source methods such as [16,29,31].

Implementation Details To train our model, we utilize the Adam optimizer [11] with 3×10^{-5} learning rate, 5×10^{-4} weight decay, 1 batch size, and 40 epochs. We use $L = 3$ layers of the MsHM and performe 20 Sinkhorn iterations. We set the hyperparameter $\beta = 10$, the raw feature channel $d = 171$, and the GH descriptor channel $D = 2048$. We use 200 subjects as the training set and 50 subjects as the test set. We implement our network using the PyTorch library [18].

Table 2. Sensitivity analysis on the proposed H^{2}GM

Weights	Accuracy (%)	Correlation	MGE
$\beta = 0.1$	77.96 ± 8.22	37.94 ± 3.91	6.3
$\beta = 1$	77.71 ± 8.24	37.90 ± 3.91	5.9
$\beta = 10$	$\mathbf{78.03 \pm 8.21}$	$\mathbf{37.99 \pm 3.91}$	**5.8**
$\beta = 100$	76.90 ± 8.30	36.92 ± 3.97	6.9

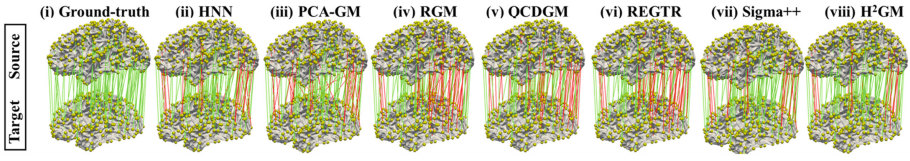

Fig. 3. Visualization of GH alignment results. The green and red lines represent the correct and incorrect alignments, respectively. (Color figure online)

3.2 Experimental Results

Comparison with State-of-the-Arts: We present the comparison results in Table 1. The accuracy, correlation, and MGE of H^{2}GM achieves $78.03 \pm 8.21\%$, $(37.99 \pm 3.91) \times 10^{-2}$, and 5.8, respectively, outperforming existing works by a large margin. Compared with learning-based approaches, showing our advantages over existing works. Besides, compared to other works, the highest correlation and the lowest MGE obtained by our proposed H^{2}GM demonstrates that our proposed framework provides the most precise GH alignment.

Ablation Studies: Table 1 displays ablation studies that verify the efficacy of each module of the proposed H^{2}GM. Our results demonstrate that inter-scale semantic consistency enhances the effectiveness of our approach, as evidenced by the removal of ISC alignment accuracy $77.66 \pm 8.27\%$. Introducing multi-scale atlases improves alignment accuracy by reducing error tolerance, as indicated by removing the two scales' brain atlas accuracy $74.81 \pm 8.66\%$. Removing the hyperedge relation learning accuracy $77.43 \pm 8.28\%$ suggests that the hyperedge structure-aware message is instrumental in improving alignment accuracy.

Sensitivity Analysis: We conduct experiments with varying hyperparameters to investigate the sensitivity of β in Eq. 8 and record the results in Table 2. Our findings indicate that the highest alignment accuracy is achieved when $\beta = 10$. However, a β setting that is too small leads to a slight performance decline due to insufficient inter-scale semantic consistency. Conversely, a β setting that is too large also leads to a performance decline.

Qualitative Analysis: Figure 3 presents the visualization results of GH alignment. Randomly selected pairs of subjects show that our method achieves the highest accuracy compared to state-of-the-art methods. These findings suggest that exploring higher-order relations between GHs can optimize GH alignment.

4 Conclusion

In this paper, we propose a novel framework H^{2}GM for brain landmark alignment. Specifically, H^{2}GM consists of a MsHE module for constructing the multi-scale hypergraphs, a MsHM module for matching them, and ISC for incorporating the semantic consistency among scales. Experimental results demonstrate that our proposed H^{2}GM outperforms existing approaches significantly.

Acknowledgment. This work was supported in part by the Innovation and Technology Commission-Innovation and Technology Fund ITS/100/20, in part by the National Natural Science Foundation of China [62001410, 31671005, 31971288, and U1801265], and in part by the Innovation Foundation for Doctor Dissertation of Northwestern Polytechnical University [CX2022052].

References

1. Avena-Koenigsberger, A., Misic, B., Sporns, O.: Communication dynamics in complex brain networks. Nat. Rev. Neurosci. **19**(1), 17–33 (2018)
2. Bai, S., Zhang, F., Torr, P.H.: Hypergraph convolution and hypergraph attention. Pattern Recogn. **110**, 107637 (2021)
3. Chen, Z., Zhang, J., Che, S., Huang, J., Han, X., Yuan, Y.: Diagnose like a pathologist: weakly-supervised pathologist-tree network for slide-level immunohistochemical scoring. In: Proceedings of the AAAI Conference on Artificial Intelligence, vol. 35, pp. 47–54 (2021)
4. Desikan, R.S., et al.: An automated labeling system for subdividing the human cerebral cortex on MRI scans into gyral based regions of interest. Neuroimage **31**(3), 968–980 (2006)
5. Feng, Y., You, H., Zhang, Z., Ji, R., Gao, Y.: Hypergraph neural networks. In: Proceedings of the AAAI Conference on Artificial Intelligence, vol. 33, pp. 3558–3565 (2019)
6. Fischl, B., Sereno, M.I., Tootell, R.B., Dale, A.M.: High-resolution intersubject averaging and a coordinate system for the cortical surface. Hum. Brain Mapp. **8**(4), 272–284 (1999)
7. Fu, K., Liu, S., Luo, X., Wang, M.: Robust point cloud registration framework based on deep graph matching. In: Proceedings of the IEEE/CVF Conference on Computer Vision and Pattern Recognition, pp. 8893–8902 (2021)
8. Gao, Q., Wang, F., Xue, N., Yu, J.G., Xia, G.S.: Deep graph matching under quadratic constraint. In: Proceedings of the IEEE/CVF Conference on Computer Vision and Pattern Recognition, pp. 5069–5078 (2021)
9. He, H., Razlighi, Q.R.: Landmark-guided region-based spatial normalization for functional magnetic resonance imaging. Hum. Brain Mapp. **43**(11), 3524–3544 (2022)
10. He, Z., et al.: Gyral hinges account for the highest cost and the highest communication capacity in a corticocortical network. Cereb. Cortex **32**(16), 3359–3376 (2022)
11. Kingma, D.P., Ba, J.: Adam: a method for stochastic optimization. arXiv preprint arXiv:1412.6980 (2014)
12. Kuhn, H.W.: The Hungarian method for the assignment problem. Nav. Res. Logist. Q. **2**(1–2), 83–97 (1955)
13. Li, K., et al.: Gyral folding pattern analysis via surface profiling. Neuroimage **52**(4), 1202–1214 (2010)
14. Li, W., Liu, X., Yuan, Y.: Sigma: semantic-complete graph matching for domain adaptive object detection. In: Proceedings of the IEEE/CVF Conference on Computer Vision and Pattern Recognition, pp. 5291–5300 (2022)
15. Li, W., Liu, X., Yuan, Y.: SIGMA++: improved semantic-complete graph matching for domain adaptive object detection. IEEE Trans. Pattern Anal. Mach. Intell. (2023)
16. Li, X., et al.: Commonly preserved and species-specific gyral folding patterns across primate brains. Brain Struct. Funct. **222**, 2127–2141 (2017)
17. Litany, O., Remez, T., Rodola, E., Bronstein, A., Bronstein, M.: Deep functional maps: structured prediction for dense shape correspondence. In: Proceedings of the IEEE International Conference on Computer Vision, pp. 5659–5667 (2017)
18. Paszke, A., et al.: Pytorch: an imperative style, high-performance deep learning library. In: Advances in Neural Information Processing Systems, vol. 32 (2019)

19. Sinkhorn, R.: A relationship between arbitrary positive matrices and doubly stochastic matrices. Ann. Math. Stat. **35**(2), 876–879 (1964)
20. Ulyanov, D., Vedaldi, A., Lempitsky, V.: Instance normalization: the missing ingredient for fast stylization. arXiv preprint arXiv:1607.08022 (2016)
21. Van Essen, D.C., et al.: The WU-Minn human connectome project: an overview. Neuroimage **80**, 62–79 (2013)
22. Vaswani, A., et al.: Attention is all you need. In: Advances in Neural Information Processing Systems, vol. 30 (2017)
23. Wang, Q., et al.: Modeling functional difference between gyri and sulci within intrinsic connectivity networks. Cerebral Cortex **33**(4), 933–947 (2022)
24. Wang, R., Yan, J., Yang, X.: Learning combinatorial embedding networks for deep graph matching. In: Proceedings of the IEEE/CVF International Conference on Computer Vision, pp. 3056–3065 (2019)
25. Wang, Y., Sun, Y., Liu, Z., Sarma, S.E., Bronstein, M.M., Solomon, J.M.: Dynamic graph CNN for learning on point clouds. ACM Trans. Graph. (TOG) **38**(5), 1–12 (2019)
26. Xu, C., Li, M., Ni, Z., Zhang, Y., Chen, S.: Groupnet: multiscale hypergraph neural networks for trajectory prediction with relational reasoning. In: Proceedings of the IEEE/CVF Conference on Computer Vision and Pattern Recognition, pp. 6498–6507 (2022)
27. Yew, Z.J., Lee, G.H.: REGTR: end-to-end point cloud correspondences with transformers. In: Proceedings of the IEEE/CVF Conference on Computer Vision and Pattern Recognition, pp. 6677–6686 (2022)
28. Zhang, S., et al.: Gyral peaks: novel gyral landmarks in developing macaque brains. Hum. Brain Mapp. **43**(15), 4540–4555 (2022)
29. Zhang, T., et al.: Identifying cross-individual correspondences of 3-hinge gyri. Med. Image Anal. **63**, 101700 (2020)
30. Zhang, T., et al.: Cortical 3-hinges could serve as hubs in cortico-cortical connective network. Brain Imaging Behav. **14**(6), 2512–2529 (2020). https://doi.org/10.1007/s11682-019-00204-6
31. Zhang, T., et al.: Group-wise graph matching of cortical gyral hinges. In: Shen, D., et al. (eds.) MICCAI 2019. LNCS, vol. 11767, pp. 75–83. Springer, Cham (2019). https://doi.org/10.1007/978-3-030-32251-9_9
32. Zhang, Z., et al.: H2MN: graph similarity learning with hierarchical hypergraph matching networks. In: Proceedings of the 27th ACM SIGKDD Conference on Knowledge Discovery & Data Mining, pp. 2274–2284 (2021)